Journal of Theoretical Biology 498 (2020) 110263

Contents lists available at ScienceDirect

Journal of Theoretical Biology

journal homepage: www.elsevier.com/locate/jtb

# The effect of viral plasticity on the persistence of host-virus systems

Melinda Choua [a], Michael R. Heath [a], Douglas C. Speirs [a], Juan A. Bonachela [b,*]

[a] Marine Population Modelling Group, Department of Mathematics and Statistics, University of Strathclyde, Glasgow, Scotland, UK
[b] Department of Ecology, Evolution and Natural Resources, Rutgers University, New Brunswick, New Jersey, United States

ARTICLE INFO

*Article history:*
Received 23 July 2019
Revised 20 February 2020
Accepted 26 March 2020
Available online 22 April 2020

ABSTRACT

Phenotypic plasticity plays an important role in the survival of individuals. In microbial host-virus systems, previous studies have shown the stabilizing effect that host plasticity has on the coexistence of the system. By contrast, it remains uncertain how the dependence of the virus on the metabolism of the host (i.e. "viral plasticity") shapes bacteria-phage population dynamics in general, or the stability of the system in particular. Moreover, bacteria-phage models that do not consider viral plasticity are now recognised as overly simplistic. For these reasons, here we focus on the effect of viral plasticity on the stability of the system under different environmental conditions. We compared the predictions from a standard bacteria-phage model, which neglects plasticity, with those of a modification that includes viral plasticity. We investigated under which conditions viral plasticity promotes coexistence, with or without oscillatory dynamics. Our analysis shows that including viral plasticity reveals coexistence in regions of the parameter space where models without plasticity predict a collapse of the system. We also show that viral plasticity tends to reduce population oscillations, although this stabilizing effect is not consistently observed across environmental conditions: plasticity may instead reinforce dynamic feedbacks between the host, the virus, and the environment, which leads to wider oscillations. Our results contribute to a deeper understanding of the dynamic control of bacteriophage on host populations observed in nature.



## 1. Introduction

Host-virus interactions can be found at any trophic level, from unicellular organisms to plants and animals. In marine ecosystems, for example, early studies revealed the importance of the mortality induced by lytic viruses on bacterioplankton (Fuhrman and McManus 1984; Servais et al. 1985; Sherr and Pedrós-Alió 1989). These viruses, known as phages or bacteriophages, infect bacteria and can kill up to 40% of the standing stock of autotrophic and heterotrophic bacteria present in the ocean each day (Fuhrman 1999). Viral lysis therefore introduces additional pathways in the microbial loop by releasing the organic and inorganic material contained in the bacterial cells (Abedon 2009; Breitbart 2012; Fuhrman and McManus 1984; O'Malley 2016). This "viral shunt" re-routes the transportation of carbon and other nutrients toward higher trophic levels (Fuhrman 1992; Bratbak et al. 1993). Characterising the dynamics of phage-bacteria interactions is therefore an essential component of the qualitative and quantitative understanding of biogeochemical cycles (Gaedke et al. 2002; Choua and Bonachela 2019).

A successful lytic phage infection starts with the encounter and irreversible attachment (i.e. adsorption) of the phage on to a specific receptor at the host surface (Calendar and Abedon 2005). The virus then inserts its genome into the host cytoplasm, and triggers the biosynthesis of viral genome and proteins by the host machinery. The host machinery (ribosomes, ATP, etc.) is thus hijacked to transcribe proteins and other components needed for the viral offspring. The lytic cycle ends when host membrane lysis occurs and the virions are released into the environment (Abedon et al. 2003). These processes define the main life-history traits of the phage (Weinbauer 2004): (i) *adsorption rate*, or number of successful viral attachments to the host per unit time; (ii) *eclipse period*, or time between attachment and the assembly of the first virion; (iii) *maturation rate*, or number of virions assembled per unit time; (iv) *latent period*, or time between adsorption and host lysis and (v) *burst size*, or number of virions released to the environment per infection. The adsorption process and rate depend on a combination of factors such as the host receptor density (Schwartz 1976; Berg and Purcell 1977) and size (Delbrück 1940), e.g. larger hosts lead to larger adsorption rates (Delbrück 1940, Rabinovitch et al. 2002). In

* Corresponding author.
*E-mail address:* juan.bonachela@rutgers.edu (J.A. Bonachela).

https://doi.org/10.1016/j.jtbi.2020.110263

addition, a larger size decreases the surface-to-volume ratio, which decreases the diffusion of nutrient through the cell membrane but increases its internal diffusion (Gallet et al. 2017), both therefore affecting the intracellular resources used by the host (and virus). The eclipse period and the maturation rate depend mainly on the host synthesis machinery and intracellular resources (Walsh and Mohr 2011; Calendar and Abedon 2005). The factors that determine the latent period remain unknown, but the number of virions assembled by the end of the latent period determines the burst size (Gnezda-Meijer et al. 2006). All else being equal, a longer latent period results in the release of more virions (Abedon 1989; Wang 2006).

All the factors above point to a dependence of viral traits (and thus performance) on the host physiological state. This dependence has indeed been observed experimentally (You et al. 2002; Rabinovitch et al. 2002; Birch et al. 2012; Golec et al. 2014). These experiments show that the eclipse and latent period decrease when the host growth rate increases, whereas the maturation rate and burst size increase. These changes in the value of viral traits are active and/or passive response of the virus to physiological changes in the host (effectively the phage's environment), and are referred to as viral phenotypic plasticity (Abedon et al. 2001; Choua and Bonachela 2019). Although many theoretical models have highlighted the importance of microbial phenotypic plasticity in their ecological interactions (Mougi and Kishida 2009; Ramos-Jiliberto et al. 2008; Hoverman 2010; Yamamichi et al. 2011; Bonachela et al. 2011; Lomas et al. 2014), for host-virus systems it remains less well studied how phenotypic plasticity shapes community and population dynamics, stability, and structure.

Few models have studied plasticity in host-virus systems; for example, analysing how the host responded plastically to viral infection through a decrease in the receptor density at the host surface (Thyrhaug et al. 2003), how host growth slowdown affects lysis (Weitz and Dushoff 2008), or how the viral plasticity affects host-virus interactions (Edwards and Steward 2018; Choua and Bonachela 2019). Host-virus models with host plasticity show that the inducible defence of the host to changing infection levels resulted in an increase of the probability of coexistence between host and phage. Models that include plasticity in viral traits revealed dramatic differences with respect to standard predictions that neglect viral plasticity. Indeed, viral plasticity affects, for example, the strength and timing of the interactions between host, virus and environment, including emergent oscillations between host and phage (Choua and Bonachela 2019). Little attention has been paid, however, to the study of the effect that viral plasticity can have on system stability and coexistence (but see Weitz and Dushoff 2008 or, regarding the stability of a nonplastic model, Beretta and Kuang 1998).

Here, we aim to understand whether viral plasticity makes coexistence between host and virus more or less likely. Specifically, we focus on understanding whether the existence of viral plasticity affects the regions of the trait- and environmental-parameter-space where coexistence is expected. To this end, we contrast the predictions from a classic host-bacteriophage model that neglects viral plasticity, with those of a version that includes viral plasticity through existing data-informed relationships between viral traits and the host growth rate (Choua and Bonachela 2019). Specifically, we compare the stability of the plastic and nonplastic versions of the most common host-phage model system (T-phage infecting *Escherichia coli*) under a diversity of host and viral traits combinations, as well as under different environmental conditions. We analyse under which conditions viral plasticity translates into an increase of coexistence between host and virus, and how it alters the oscillations typically observed for antagonistic interactions.

## 2. Methods

### 2.1. Model description

We represented the ecological dynamics of the host-phage system using a modified version of a well-known model that has been validated by experiments (Levin et al. 1977). The original model explicitly represents the viral latent period, which introduces a delay between host infection and lysis. The model keeps track of the dynamics of nutrient ($N$), uninfected host ($C$), and virus ($V$). The environmental conditions are assumed to be those of a chemostat, a well-stirred controlled environment in which the host and phage encounter each other randomly. It is further assumed that multiple infections do not occur, and the host machinery is used entirely for viral replication (and thus nutrient uptake and host growth stop upon infection). The latter implies that the latent period is not limited by the host's generation time. In addition, we introduced the effective influence of intraspecific competition on population growth. As bacteria grow in a limited volume (the chemostat), boundary effects can limit the space around cells as the population increases, triggering competition for space, light, or other resources not explicitly modelled here. We assumed this crowding effect to originate mostly from resource competition, which only affects uninfected hosts as uptake and growth stop at infection. This density-dependent term is often characterized by a quadratic loss term, which has the advantage of preventing or damping oscillations, thus increasing the possibility to reach stability for the system with and without plasticity (Gibert and Delong 2015). These assumptions lead to the following delay differential equations:

$$\frac{dN(t)}{dt} = w(N_0 - N) - \mu(N, r)\ C/Y \tag{1}$$

$$\frac{dC(t)}{dt} = \mu(N, r)\ C - k(r)\ C\ V - w\ C - \alpha\ C^2 \tag{2}$$

$$\frac{dV(t)}{dt} = B(\mu)\ k(r)\ C_{t-L}\ V_{t-L}\ e^{-wL} - k(r)\ C\ V - m\ V - w\ V \tag{3}$$

(see definitions of symbols and units in Table 1). The original model also considered the dynamics of the infected host population, $I(t)$; however, since using an explicit time lag suffices to capture the full dynamics of both infective viruses and susceptible hosts, we omit the equation for $I(t)$ here without any loss of generality. The first equation represents the dynamics of the nutrient concentration within the chemostat, with an inflow and outflow of nutrient (first term) and the uptake of nutrient by the host (second term). The second equation describes the growth of the free host population as a result of bacterial reproduction (first term), reduced by infection events (second term), dilution (third term) and crowding (fourth term). The lysis of infected cells produces free phages (first term of the last equation, where $e^{-wL}$ is the probability for infected cells to not be removed from the system during the latent period); the phage population can also decrease due to viruses infecting healthy hosts (second term), natural mortality (third term), and dilution (last term). These equations are purely deterministic, and variables and trait values represent the average behaviour at the population level.

The host grows following the Monod model (Monod 1949):

$$\mu(N, r) = \mu_{\max}(r)N/(N + K_n) \tag{4}$$

where $\mu_{\max}$ (maximum growth rate) and $K_n$ (half saturation constant for growth) characterize, respectively, the maximum growth potential and the inverse of the affinity of the bacteria for the limiting nutrient, $N$.

**Table 1**
Symbols for variables used in the model and parameter values

| Symbol | Description | Units | Value | References |
|---|---|---|---|---|
| $N$ | Dissolved Inorganic Nutrient Concentration | mol $l^{-1}$ | Ecological variable, Eq. (1) | (Levin, Stewart, and Chao 1977), for the equations |
| $C$ | Non-infected Host Concentration | cell $l^{-1}$ | Ecological variable, Eq. (2) | |
| $V$ | Free Virus Concentration | cell $l^{-1}$ | Ecological variable, Eq. (3) | |
| $\mu$ | Non-infected Host population Growth Rate | $d^{-1}$ | Ecological variable, Eq. (4) | (Monod 1949), for the equation |
| **Host parameters/traits** | | | | |
| $r$ | Equivalent spherical radius | µm | 0.3 – 1.1 | (Loferer-Krößbacher, Klima, and Psenner 1998) |
| $\mu_{max}$ | Maximum Host Population Growth Rate | $d^{-1}$ | Eq. (5) | (Gallet et al. 2017) |
| $c$, $h$ | Parameters Eq. (5) | – | f=0.33 p=3.8 | (Gallet et al. 2017) |
| $K_{ref}$ | Half-Saturation constant for $\mu_{max} = 0$ | mol $l^{-1}$ | $3.05 \times 10^{-8}$ | (Wirtz 2002) |
| $\mu_{ref}$ | Asymptotic $\mu_{max}$ for $K_n \to \infty$ | $d^{-1}$ | 32.4 | (Wirtz 2002) |
| $K_n$ | Half-Saturation Constant for Growth | mol | Eq.(6) | (Wirtz 2002) |
| $Y$ | Yield Parameter | cell $mol^{-1}$ | $9 \times 10^{13}$ | (Choua and Bonachela 2019), calculated from several sources |
| $\mu_{max\ experiment}$ | Maximum Growth Rate in the experiment | $d^{-1}$ | 40.8 | (You, Suthers, and Yin 2002) |
| $\alpha$ | Parameter of crowding effect | l $d^{-1}$ cell$^{-1}$ | $0 - 12 \times 10^{-7}$ | Sensitivity analysis |
| **Viral parameters/traits** | | | | |
| $D$ | Diffusion of Viral Particle | $m^2\ s^{-1}$ | $4.3132 \times 10^{-12}$ | Calculated using Stokes-Einstein expression |
| $k$ | Adsorption Rate | l cell$^{-1}$ $d^{-1}$ | $4\pi$ D $Conv_3$ r | (Delbrück 1940) |
| $E(\mu)$ | Eclipse Period | d | Eq. (8) | (Choua and Bonachela 2019) |
| $M(\mu)$ | Maturation Rate | virions $d^{-1}$ | Eq. (9) | (Choua and Bonachela 2019) |
| $L$ | Latent Period | d | 0.01 - 1 | (You, Suthers, and Yin 2002, Golec et al. 2014) |
| $B$ | Burst Size | virions cell$^{-1}$ | B = M (L-E) | (Wang 2006) |
| **Chemostat parameters** | | | | |
| $w$ | Chemostat Dilution Rate | $d^{-1}$ | 1 - 30 | Ranges set by Eq. (6) and range for $r$ |
| $N_0$ | Dissolved Inorganic Nutrient Supply Concentration | mol $l^{-1}$ | $9 \times 10^{-5}$ | Sensitivity analysis |
| **Conversion factors** | | | | |
| $Conv_1$ | Constant to convert from (ml) to ($\mu m^3$) | $\mu m^3 ml^{-1}$ | $10^{-12}$ | – |
| $Conv_2$ | Constant to convert from ($hour^{-1}$) to ($d^{-1}$) | hour $d^{-1}$ | 24 | – |
| $Conv_3$ | Constant to convert from ($m^3\ s^{-1}$) to (l $d^{-1}$) | l s $d^{-1}$ $m^{-3}$ | $86400 \times 10^3$ | – |

#### 2.1.1. Host trait set

Although our approach can be generalised to any bacterium, we parameterized the host according to E.coli. This choice also allowed us to find allometries and relationships linking host traits thus reducing the dimensionality of the parameter space. We focused on host size as the main trait characterising hosts. Cell size is a "master" trait for most microorganisms including bacteria, i.e. most other host traits depend on size (Litchman et al. 2007). For example, the size of the host affects the surface-to-volume ratio, which changes the diffusion of nutrient from the environment through the cell's membrane, thus altering the uptake rate (external diffusion) as well as the molecular transit time inside the cell (internal diffusion) (Gallet et al. 2017); for bacteria, transit time is the limiting factor, which leads to a positive correlation between cell size and metabolic rate (Gallet et al. 2017). Specifically, experimental work provides an allometric expression linking the radius of the bacterium (assumed spherical), $r$, and its maximum potential for growth, $\mu_{\max}$ (Gallet et al. 2017; Shestopaloff 2016):

$$\mu_{\max}(r) = \mathrm{Conv}_2\ 10^{c\ log_{10}(4\pi \mathrm{Conv}_1 r^3/3)+h} \tag{5}$$

(see Table 1 for symbols and units) where the $c$ and $h$ parameters determine how steeply the metabolic rate increases with $r$. In turn, the two Monod traits, $\mu_{\max}$ and $K_n$, are positively correlated, which can be mathematically expressed through the following function (Wirtz 2002):

$$K_n(\mu_{\max}) = K_{ref}\ e^{\mu_{\max}(r)/(\mu_{ref}-\mu_{\max}(r))} \tag{6}$$

where $\mu_{ref}$ represents the asymptotic maximal growth rate for an infinitely high $K_n$ and $K_{ref}$ represents half-saturation constant at $\mu_{\max} = 0$. The exact shape of this positive relationship does not affect qualitatively our results (see Appendix).

#### 2.1.2. Phage trait set and plasticity

We focused on the most dominant bacteriophage, the family Caudovirales (Calendar and Abedon 2005), and more specifically the T-phage subfamily. The receptors that these viruses use to infect their host (predominantly E.Coli) occupy up to 75% of the cell surface (Nikaido and Vaara 1985), which allowed us to assume that each collision leads effectively to adsorption (Berg and Purcell 1977; Schwartz 1976; Delbrück 1940). The size of the host, nonetheless, affects the viral adsorption rate, which has been represented in the past using the linear function $k = 4\pi rD$ (Delbrück 1940), where $D$ is the diffusion coefficient of the phage.

Because the exact factors that determine the latent period, $L$, are unknown (Wang et al. 2000; Ramanculov and Young 2001; Young and Bläsi 1995), we used here the latent period as a free parameter characterizing the virus. The burst size, $B$, depends on the number of phages that has been assembled during the infection time. We assume that the time needed to deplete host resources involved in intracellular phage production is much larger than the latent period, and therefore the offspring number is only limited by lysis. This assumption is typically represented by the linear function $B = M(L - E)$ (Wang 2006), where $E$ and $M$ represent the eclipse period and maturation rate. $E$ and $M$, in turn, depend on the physiological state of the host (e.g. host growth rate, $\mu$). In order to account for this dependence, we used the following data-informed expressions (Choua and Bonachela 2019):

$$E(\mu_n) = E_\infty + E_0 e^{-\alpha_E \mu_n} \tag{7}$$

$$M(\mu_n) = \frac{M_\infty}{1 + e^{\alpha_M(\mu_n - M_0)}} \tag{8}$$

where $\mu_n$ is a normalized version of the host growth rate (see Appendix A for further details). These functional forms represent a decreasing exponential and a sigmoid function, respectively. Note that, following experimental observations (Golec et al. 2014), Eq. (7) shows a finite eclipse period even for $\mu \to 0$, effectively allowing viral reproduction at very low host growth rates. Another possibility for such extreme conditions may instead be a change in strategy of the virus, switching from lytic to temperate (e.g. lysogenic) mode. Although other modelling efforts have delved into the conditions leading to the switch between modes factoring in the physiological state of the host (Wang and Goldenfeld 2010), our model focuses on purely-lytic viruses and, hence, we did not include this possibility in our description. Both func-

tional forms above show a plateau at high growth rates, which reflects the physiological limit of the host machinery to synthesizing proteins (Choua and Bonachela 2019). $E_\infty$ and $E_0$ determine $E$ for very low growth rates, and $\alpha_E$ determines the slope of the (decreasing) function; $M_\infty$ represents the upper plateau of the sigmoid, $\alpha_M$ how steeply $M$ reaches it, and $M_0$ the midpoint of the sigmoid. These expressions enable a plastic description of the burst size:

$$B(\mu_n) = M(\mu_n)(L - E(\mu_n)) \tag{9}$$

The equation above follows the observation that burst size and latent period are linearly related (Wang 2006), and assumes that the virus is not necessarily limited by the recycling of host material but can also synthesize certain components de novo (e.g. viral nucleotides Maat et al. 2016). As a consequence, burst size is only limited by the duration of infection and assembly rate.

Thus, Eqs. (1)–(3) were integrated numerically for 200 days, which enabled reaching a stationary state for the main variables. Host size (and therefore maximum growth rate and half-saturation constant, Eqs. (5) and (6)) were set from the outset, whereas viral traits (i.e. $E(\mu_n)$, $M(\mu_n)$, and thus $B(\mu_n)$) were adjusted at each integration step to follow updates in the host growth rate.

On the other hand, models that neglect viral plasticity use fixed values for $E$ and $M$. These values are usually obtained from experiments that standardly set optimal conditions for the host. In consequence, the associated $E_{non}$ and $M_{non}$ reflect the performance of the host machinery at $\mu = \mu_{\max}$. These values are host-specific: because different host phenotypes/strains will show different sizes and therefore different $\mu_{\max}$, $E_{non}$ and $M_{non}$ must vary accordingly. We could not find values for $E$ and $M$ for all the different host sizes used in our simulations, and thus we estimated those values as $E_{non} = E(\mu_n = 1)$ and $M_{non} = M(\mu_n = 1)$ (see Eqs. (7) and (8), and further details in Appendix A). In consequence, the burst size for the nonplastic virus follows the expression below:

$$B_{non} = M_{non}(r)(L - E_{non}(r)) \tag{10}$$

*2.1.3. Analysis*

The model described above has four main parameters for which there is limited amount of information available and/or a large associated variability: the host radius, $r$; the viral latent period, $L$; the crowding strength, $\alpha$; and the dilution rate, $w$ (the latter represents environmental conditions). These four parameters defined our parameter space. Table 1 shows their range of variation. The range for the host radius provided trait values (volume, $\mu_{\max}$ and $K_n$, through Eqs. (5) and (6)) compatible with experimental observations Füchslin et al. 2012; Schulze and Lipe 1964; Loferer-Krößbacher et al. 1998). We discretised this interval in 41 sections to obtain a computationally reasonable resolution for the $r$ axis. The range for the latent period covered 22 realistic values for T-phages. The dilution rate was incremented by $1d^{-1}$ until reaching the maximal growth rate possible limited by either the host size (i.e. $\mu_{\max}(r)$) or nutrient availability (i.e. $\mu(N_0)$). Above these values, bacterial growth cannot overcome dilution providing thus analytical limits of coexistence (i.e. Eq. (2) constantly negative due to $\mu < w$) ultimately leading to extinction. Finally, the range for the crowding strength is to provide a crowding terms that show values comparable to the rest of terms in Eq. (2).

To analyse the stability of the ecological interactions (Eqs. (1)–(3)) in the parameter space $(r, L, w, \alpha)$, we used Matlab to calculate the stationary states/cycles obtained with the model for each parameter combination. We then classified these outputs into one of these 3 categories: (i) "no coexistence between bacteria and viruses", (ii) "coexistence with oscillations", and (iii) "coexistence without oscillations". "No coexistence" occurred when the population of either the host or the virus fell below the threshold of one individual per litre. This threshold avoids an unrealistic recovery of effectively-extinct populations. To detect non-oscillatory coexistence, we checked if the difference between the last value of the simulation and two other previous points separated in time by 1 and 2.3 days (i.e. $10^4$ time steps) provided a similar value.

Finally, to compare the outcomes above with the predictions for a nonplastic virus, we repeated this analysis with $E = E_{non}$ and $M = M_{non}$. Although analytical expressions can be calculated for the nonplastic case, a closed expression cannot be obtained for the plastic case due to the dependence of $E$ and $M$ on $\mu(N)$. Therefore, for the sake of consistency, we used numerical simulations of the model for both plastic and nonplastic cases.

*2.1.4. Dimensionality of the parameter space*

After we classified the outcomes of all the combinations of the four parameters $(r, L, w, \alpha)$, we proceeded to reduce the dimensionality of the parameter space. To this end, we first selected a fixed value for $\alpha$. Because density-dependence typically helps to stabilize oscillations, the expectation is that this term will contribute to widen the region of the parameter space where coexistence occurs. Thus, for each value of $\alpha$ we counted the number of cases that showed coexistence (with and without oscillations) in both the plastic and the nonplastic cases to focus on those $\alpha$ that provided the highest number of cases showing coexistence. This term, however, should not overwhelmingly regulate the dynamics. Therefore, to ensure that the system remains regulated by the host-virus interaction and not by intraspecific competition solely, we selected the $\alpha$ that provided the highest number of cases where the ratio between viral mortality and intraspecific competition was above one (i.e. $k\ C_{st}\ V_{st}/(\alpha\ C_{st}^2) > 1$, where the subscript "$st$" refers to the value obtained by averaging the last 20 days of the simulations that reached a stationary state).

Fixing $\alpha$ reduced the parameter space to 3 dimensions $(r, L, w)$. Simulations for all possible combinations of these three parameters allowed us to analyse the resulting manifold. Specifically, we focused on understanding (i) the boundary between the area of general coexistence and no-coexistence, (ii) the areas where plastic viruses show coexistence but nonplastic viruses do not, and (iii) vice-versa. To this end, we compared the results obtained for different $L$ (i.e. specific slices of the manifold). We also focused on particular host radii in order to explore the role of environmental conditions (represented by the dilution rate, $w$). To quantify whether plasticity makes coexistence more likely, we calculated the percentage of cases where either variation of the model was the only one showing coexistence with the host. Finally, to analyse the effect of plasticity on the emergence of oscillations and underlying mechanisms, we studied the population dynamics observed in the "coexistence with oscillations" cases.

## 3. Results

### 3.1. Selection of the crowding strength parameter, $\alpha$

For different values of $\alpha$, we counted the number of cases for which coexistence is found (with and without oscillations) among all the combinations of $(r, L, w)$. Within these cases of coexistence, we also counted the number of cases in which the dynamics were dominated by viral mortality over crowding (i.e. $k\ C_{st}\ V_{st}/(\alpha\ C_{st}^2) > 1$). Fig. 1 shows the increase in the frequency of simultaneous coexistence (i.e. both host and virus surviving for plastic and nonplastic cases). This persistence of the host-phage system increases with $\alpha$ until a certain value, then decreases. The frequency of coexistence when crowding is considered is up to 7 times higher than for $\alpha = 0$. A value $\alpha = 60 \times 10^{-9}$l cell$^{-1}$d$^{-1}$ optimizes the coexistence between bacteria and viruses for both plastic and nonplastic examples, and the percentage of cases regulated by viruses is

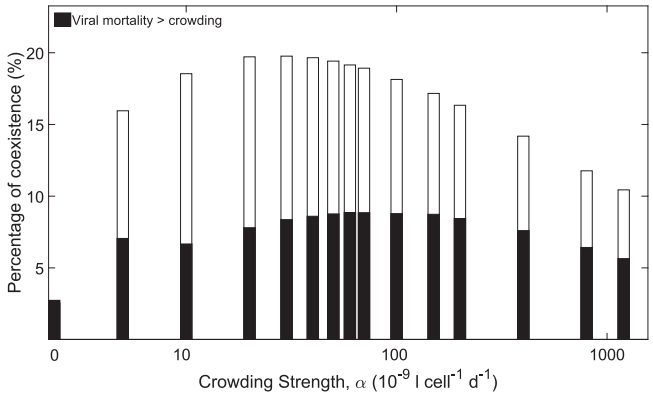


**Fig. 1.** Percentage of cases among all combinations of ($r$, $L$, $w$) that show coexistence in both plastic and nonplastic cases (white bars) for different values of $\alpha$. The black bars represent the percentage of cases, within these cases of coexistence, where viral mortality overcomes crowding in plastic and nonplastic cases.

also at its peak value. Thus, we fixed the crowding strength to this value for the rest of the analysis.

### 3.2. Exploration of the $(r, L, w)$ space

The outcome of comparing plastic and nonplastic models in the $(r, L, w)$ space formed a 3D manifold. For a better visualisation, we did not represent the cases where both plastic and nonplastic do not show coexistence (Case 1 in the following figures). The resulting manifold showed a consistent pattern that appears along the latent period axis (see Fig. C.1). To further investigate this pattern, we explored slices of the manifold across the latent period axis (in Fig. 2, $L = 0.07\ d$, $L = 0.47\ d$ and $L = 0.87\ d$). For a fixed latent period, the region of coexistence (with and without oscillations) starts at low-to-intermediate host radii and increases with $r$, becoming narrower at higher host sizes. As the latent period increases, the coexistence region is constrained to smaller dilution rates. We can differentiate four different areas of "no coexistence" in Fig. 2 attending to the reasons for the lack coexistence. In the bottom area (delineated by a dark blue dashed line) the host growth rate at the stationary state is smaller than the per-capita mortality rate induced by viruses, which drives the bacterial population to extinction (followed by the viral population). This border, constrained to low $w$, reaches higher dilution rates for intermediate host radii. The sharp decrease for host radii larger than 1 µm coincides with the area where only the plastic case shows coexistence (downward triangles and hexagrams). In the area immediately above the coexistence area (i.e. above the purple dashed line), the viral growth rate (i.e. per-capita change in the concentration of free virus, $\mu_{viral} = (Be^{-wL} - 1)\ k(r)\ C_{st}$) cannot overcome dilution, which leads to viral extinction and the thriving of the bacterial population. Overall, this area of viral extinction increases as the latent period increases, and the bacterial population survives alone unless limited by the available nutrient (grey dotted line) or by its own physiological limits (black line). In these two cases, bacterial growth cannot overcome mortality due to dilution.

We also quantified the percentage of cases of coexistence between virus and host exclusive to one or the other version of the model. The ratio between the area where only plasticity leads to coexistence and the sum of all cases with exclusive coexistence (i.e. *(number of instances that Case 2 or 3 have been observed)/(number*

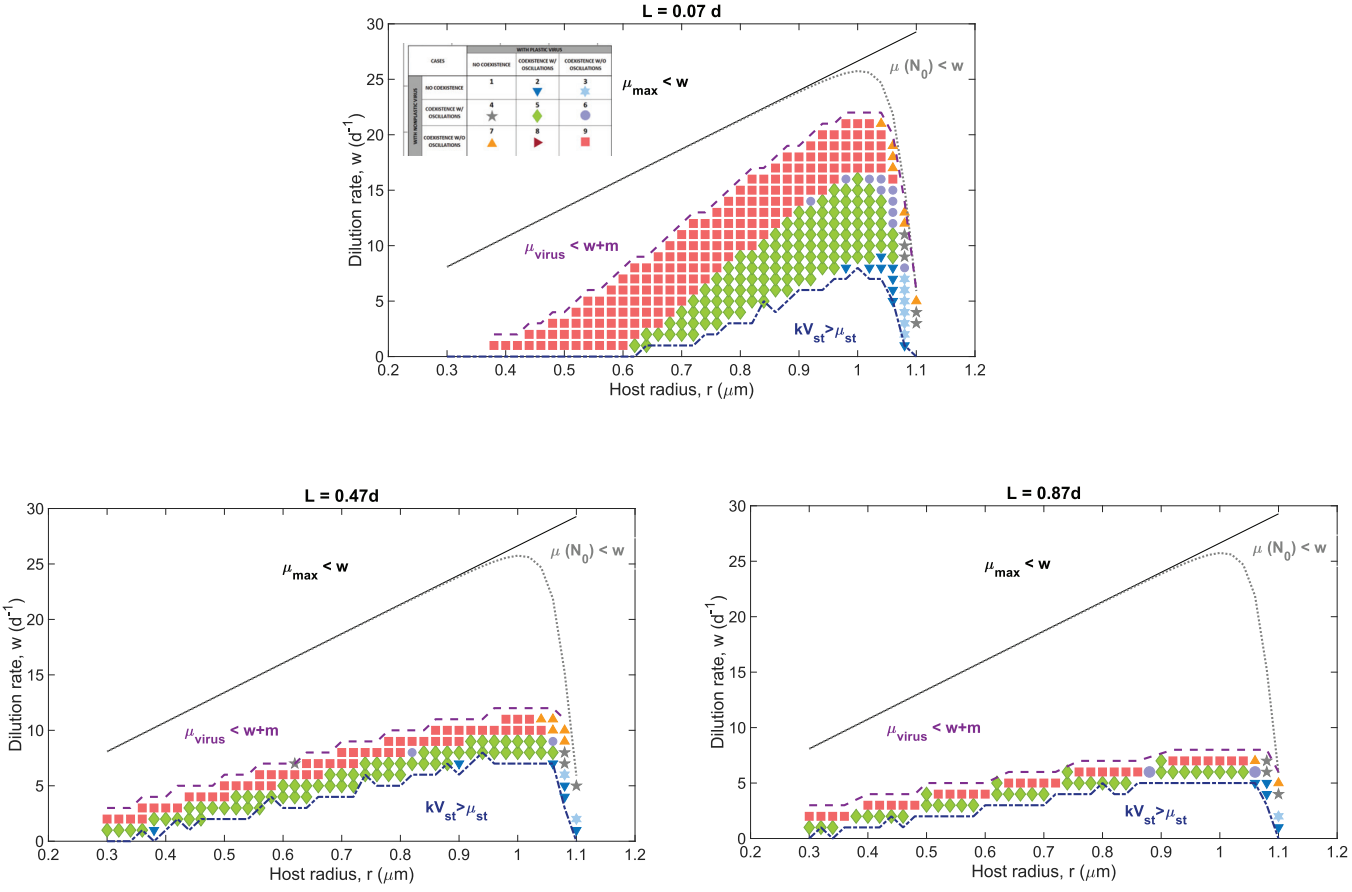


**Fig. 2.** Slices across the ($r$, $L$, $w$, $\alpha$) space, specifically for L=0.07d (top), L=0.47d (bottom left) and L=0.87d (bottom right), where the borders between coexistence and non-coexistence explicitly appear. The legend of each symbol/colour is represented in the Table inset of the top panel. See Fig. C.2 for versions of the upper panel obtained for different crowding strenghts. Color version online.

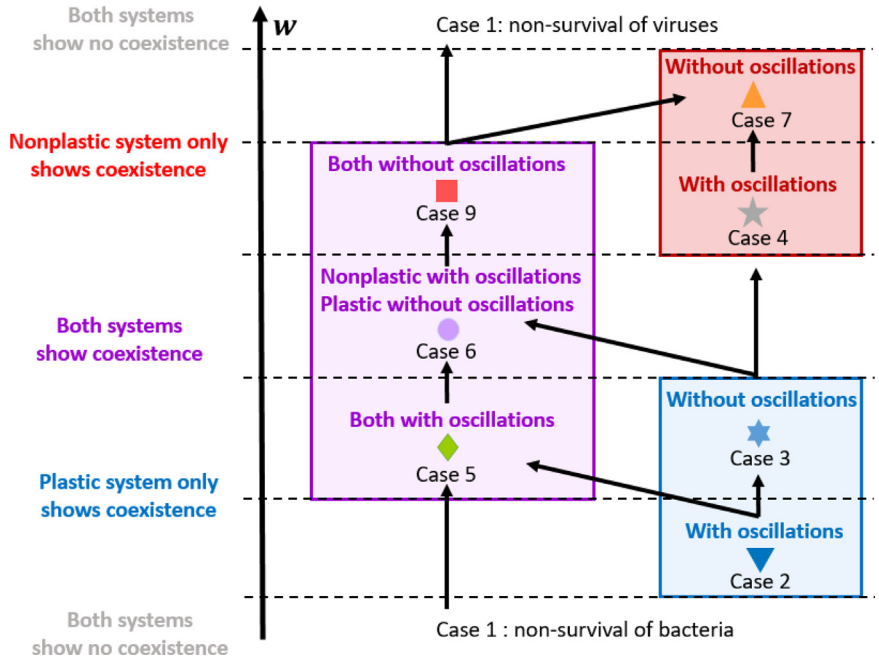


**Fig. 3.** Schematic diagram of the multiple paths that the system can follow when the dilution rate ($w$) increases, within the different combinations of parameters ($r$, $L$, $\alpha$). Note that any path can start by and/or end-up in case 1 without passing by other intermediary cases (e.g. case 5 can go directly to the upper case 1). Color version online.

*of instances Cases 2, 3, 4 or 7 have been observed)*, considering all latent periods) indicates that the plastic virus shows exclusive coexistence 66.92% cases, versus 33.08% for the nonplastic virus for the selected $\alpha$. Fig. 3 summarises schematically the multiples transitions between non-coexistence and coexistence, and between the various coexistence states observed in Fig. 2 as the dilution rate changes.

Fig. 3 shows that only the plastic description of the model shows coexistence for low dilution rates (cases 2 and 3, typically observed for high host sizes, see Fig. 2 and Appendix A), while only the nonplastic virus coexists with its host for higher dilution rates (cases 4 and 7). The area where the host cannot coexist with the virus (case 1 at the bottom) is smaller when the virus is plastic than when it is nonplastic (i.e. smaller dilution rates required for cases 2 than for case 4), and the area where the bacteria thrive alone (i.e. case 1 at the top) is bigger in the plastic case. Oscillatory behaviour (i.e. limit cycles) occurs at low dilution rates, then becomes a stable equilibrium as $w$ increases. This shift happens for smaller $w$ in the plastic case, and then (i.e. for larger $w$) in the nonplastic case (cases 5, 6 and 9). We never observed cases where the plastic system showed a limit cycle and the nonplastic system a stable equilibrium (case 8). When both plastic and nonplastic descriptions of the model show oscillations (case 6), the relative difference in amplitude of the oscillations in the system with the plastic virus is always smaller than in the system with the nonplastic virus (see Fig. C.3). Altering the positive relationship between the maximum growth rate and half-saturation constant (Eq. (6)) did not alter this sequence of behaviours, although the coexistence area can shift towards larger or smaller values (and therefore some of the observed behaviour can be lost if the host ranges used for e.g. Fig. 2 are not increased consequently, see Fig. B.2).

## 4. Discussion

Viral reproduction depends intrinsically on the physiological state of the host. As shown experimentally, this dependence translates into changes of viral trait values (phenotypic plasticity) when the host growth rate changes. When included in models for lytic viruses, this viral plasticity leads to important ecological and evolutionary differences with respect to standard models, which neglect viral plasticity (Edwards and Steward 2018; Choua and Bonachela 2019). Here, we focused on understanding how viral plasticity alters possible coexistence and dynamics between host and virus for a phage-bacteria system.

### 4.1. Influence of crowding and latent period on the stability of the system

The addition of a density dependent term generally contributes to dampening oscillations in models for antagonistic interactions (Gibert and Delong 2015), and this was indeed the case in our bacteria-phage system. The selected value $\alpha = 60 \times 10^{-9} l\ cell^{-1} d^{-1}$ maximized the coexistence area of the system regulated by viruses but did not affect the rest of our results qualitatively. At low $\alpha$, an increase in the crowding strength leads to an increase in coexistence. This is due to the reduction of bacterial population, which results in a decrease in the nutrient competition that helps the bacteria to survive in conditions where smaller $\alpha$ would lead to extinction. Beyond a certain value of the crowding strength, however, mortality cannot be compensated by the higher nutrient availability and persistence declines. Indeed, because $\alpha$ directly affects the bacteria, and the viruses only indirectly, the border delimiting the bacterial survival (i.e. bottom border in Fig. 2) shifts to lower dilution rates faster than the border delimiting the viral survival (i.e. upper border) as $\alpha$ increases. This "lag" between the movement of the bottom and upper borders of the coexistence region widens the region in between (i.e. the area of coexistence), which facilitates the identification of the variety of dynamics shown in Appendix C. We also noticed the increase of the region where the host survives alone (i.e. the area in between the black line and the purple dotted line in Fig. 2) as $\alpha$ increases, which raises the question of whether challenging environmental conditions that slow down bacterial growth or increase mortality may entail the counter-intuitive benefit for the bacteria of avoiding the virus.

Our results also reveal the effect of viral traits on the stability of the system. The latent period reflects the time that the virus

spends inside the host producing virions, but also the loss of opportunities to establish parallel infections. These two factors are in turn influenced by the dilution rate: a high $w$ increases the infected-cell removal but also leads to higher host density due to the increased resources in the chemostat. Small $L$ entailed coexistence for areas with high $w$, while these same areas switched to no-coexistence status when $L$ increased. The reason is that the increase in host density linked to high dilution rates provides the viral offspring with more opportunities to establish subsequent infections, and thus the virus can afford an earlier termination of infection (i.e. smaller $L$ values). These results are in line with previous studies (Abedon 1989; Choua and Bonachela 2019) that reported that both the host cell density and the infected-cell removal rate play a role in the selection of the latent period.

### 4.2. Influence of the environment (i.e. w and N) on persistence

Overall, including plasticity promoted coexistence in our *in silico* experimental setup. Fig. 3 summarizes our results and, together with Figs. 2 and C.1, highlights the cases where viral plasticity enables coexistence while the classic model does not, as well as the cases where the nonplastic model shows exclusive coexistence. Because the nonplastic virus, defined here as one with the best possible viral trait values (Eqs. (A.3) and (A.4)), can lead to a much-increased viral population, it can show coexistence in regions located close to the limit where plastic viruses cannot overcome dilution (i.e. above the purple dashed line in Fig. 2). For the plastic virus to survive in this area of the parameter space, however, the host must approach its maximum growth rate. The latter, appears to be the case for smaller host sizes in our simulations, whereas hosts with a size above 1μm cannot reach this maximal growth limit for $N \leq N_0$ (see Appendix B). This limitation forces these larger hosts to grow at a rate far from their maximum, which results in significant differences between the viral trait values of the plastic and nonplastic descriptions. The plastic virus, responding to changes in the host growth rate, shows a decrease in performance for hosts that grow slowly, allowing for the survival of these hosts and thus the coexistence of the system where the nonplastic description leads to extinction. Because in nature maximal growth rates are not easily reached by the microbial host (Maat et al. 2016), viral performance may typically be overestimated in standard models neglecting plasticity. The (more realistic) plastic representation of the virus predicts that stable coexistence between host and virus could be more widespread than expected from current models. This idea is reinforced by the fact that exclusive coexistence by the plastic virus emerges when the effects of plasticity are more noticeable, i.e. for large host sizes (see Appendix A).

### 4.3. The role of plasticity on the amplitude of emerging oscillations

In previous analyses of nonplastic host-virus models, oscillations emerge as a result of an increase in the (fixed) burst size (Beretta and Kuang 1998). In both plastic and nonplastic versions of our model, stable nodes are transformed into stable oscillations when the dilution rate increases. Our work thus generalizes the previous result by showing that host availability and viral performance, both affected by environmental conditions, are responsible for the transition from stable node to limit cycle. For cases where both plastic and nonplastic description show coexistence, the amplitude of the limit cycles occurring with plastic viruses was always smaller than these for those occurring in the nonplastic case. The differences in behaviour observed for the bacterial population are mainly localised to the bottom of the oscillations, while the top varies less (see Fig. C.3). Because the nonplastic case describes a virus always at its highest performance, the top-down pressure on the host is higher, which decreases the bacterial population to a level lower than the plastic virus (sometimes driving the host to extinction). When the host survives, fewer bacteria compete for nutrient in the lower part of the oscillation and we might expect the bacterial population to reach a higher maximum than in the plastic case. However, this effect is dampened when bacterial growth reaches its largest possible value (i.e. $\mu \approx \min(\mu(N_0), \mu = \mu_{\max})$).

Viral plasticity may not dampen the system's population-level oscillations, however, if there is an additional source of free hosts available in the environment. As described above and in (Choua and Bonachela 2019), low host growth leads to a reduced viral performance, which translates into host population densities that are higher than the expectation from a system with a nonplastic description of the virus. In systems with an additional source of fresh hosts (e.g. two-stage chemostats), this effect is reinforced for low resource and host input rates (see right panel Fig. C.4). In these cases, the additional hosts help compensate the lower viral production (due to the lower host growth rate) shown by the plastic virus with a higher infection rate. As a consequence, the viral population reaches higher maximal values (oscillation tops) than in the nonplastic description. This increased population of plastic virus subsequently draws down the bacterial population to a value (oscillation bottoms) that is similar or even lower than in the nonplastic case, which in turn facilitates the recovery of N, reinitializing a cycle that results in larger amplitudes for the plastic oscillatory dynamics (Choua and Bonachela 2019). This feedback effect, however, is not observed with our current setup in which there is no external source of hosts.

## 5. Conclusions

Previous studies have suggested that viruses limit the development of phytoplankton blooms (Brussaard 2004). Although host availability is known to be an important factor influencing viral regulation, it is still unclear how exactly viruses regulate the host population in nature, and when and how viruses can prevent blooms from happening (Brussaard 2004; Suttle 2007; Choua and Bonachela 2019). A previous study that considered host plasticity showed that the feedback between host and virus accentuates the decrease of viral pressure when the host availability is decimated by viral lysis (Thyrhaug et al. 2003). However, to fully comprehend the impact of viral control on host populations it is essential to identify factors that affect viral infection and replication, which we know depend on the metabolism of the host (Brussaard 2004; Choua and Bonachela 2019). As we show in this study, the inclusion of viral plasticity may help to this end.

Our study reveals a subtle interplay between host, virus and environment. The flexibility of the viral traits conferred by plasticity can increase the probability of coexistence between host and phage and, for environments like the chemostat used here, reduce the amplitude of emerging population-density oscillations. If an external source of free hosts is available, however, plasticity can under certain circumstances reinforce the feedbacks between the system and the environment, leading to wider oscillations. In addition, the fact that the plastic virus "accommodates" its performance to the physiological state of the host provides the latter with relief from a top-down pressure that would drive it to extinction if the virus just kept a maximal performance. As a result, plasticity enables coexistence in regions of the parameter space where the standard version of the model, which neglects plasticity, predicts a collapse of the system. The cases where only the nonplastic case shows coexistence, on the other hand, should be considered with caution, as the high performance of the virus imposed in nonplastic models keeps the viral population artificially alive. Moreover, the plastic virus can drive the bacterial population to either lower or higher

abundances than the nonplastic case (in which viral dynamics are entirely regulated by host availability) depending on the balance between host availability and host physiological state, which captures some of the multiple facets of viral control observed in nature. Additional experimental information regarding how different environment factors regulate viral dynamics and host-virus interactions are required to generalize our theory. In addition to the potential technical difficulty, obtaining some of this information may be challenging because, in many cases, such factors are unknown (e.g. the mechanisms that trigger a switch between lytic and temperate infection, as some viruses may show either mode). Incorporating explicitly aspects such as viral dynamics and plasticity into global biogeochemical models could significantly improve their predictability, but still remains a big challenge (Choua and Bonachela 2019).

## Author contribution statement

M.C., M.R.H., D.C.S., and J.A.B. designed research; M.C. performed research; M.C., M.R.H., D.C.S., and J.A.B. wrote the manuscript.

## Acknowledgments

We would like to thank K. Edwards for helpful discussions in the early stages of this study. M.C. and J.A.B. were supported by the Marine Alliance for Science and Technology for Scotland pooling initiative, funded by the Scottish Funding Council (HR09011) and contributing institutions.

## Appendix

### A. Utilisation of functional forms to express viral traits

The parametrisation of the functional forms we use here to represent viral plasticity Choua and Bonachela 2019) is based on experiments for *E.Coli* that can reach a maximal growth rate of 40.8 $d^{-1}$ ($\mu_{\max experiment}$). At this growth rate, the performance of the host machinery is very high, which is reflected on the viral traits ($E$ and $M$). In this paper, however, we model different sizes for the host cell and, because their $\mu_{\max}$ is limited by size through Eq. (5), the host growth rate cannot reach $\mu_{\max experiment}$. For this reason, in order to stay consistent with the experiments, the normalized growth rate ($\mu_n$) that appears in Eqs. (7) and (8) is based on $\mu_{\max experiment}$, leading to the expressions:

$$E(\mu) = E_\infty + E_0 e^{-\alpha_E \ \mu/\mu_{\max,experiment}} \tag{A.1}$$

$$M(\mu) = \frac{M_\infty}{1 + e^{\alpha_M(\mu/\mu_{\max,experiment} - M_0)}} \tag{A.2}$$

As with standard models, the nonplastic version of the model uses fixed viral trait values ($E_{non}$ and $M_{non}$) obtained for a host grown under optimal conditions (i.e. $\mu = \mu_{\max}$) (Choua and Bonachela 2019). These values are thus host-specific and, therefore, as $\mu_{\max}$ changes with host size ($\mu_{\max}(r)$), $E_{non}$ and $M_{non}$ change accordingly as well:

$$E_{non}(r) = E_\infty + E_0 e^{-\alpha_E \mu_{\max}(r)/\mu_{\max,experiment}} \tag{A.3}$$

$$M_{non}(r) = \frac{M_\infty}{1 + e^{\alpha_M(\mu_{\max}(r)/\mu_{\max,experiment} - M_0)}} \tag{A.4}$$

With this description, the range of variation of the plastic viral traits increases with the size of the host, thus allowing the effect of plasticity to be more noticeable for higher host sizes (see Fig. A.1).

### B. Role of the expression for the substrate affinity

Fig. B.1 shows the effect of the size on the host growth rate. Because of the relationship between $\mu_{\max}$ and $K_n$ (Eq. (6)) and the allometric function $\mu_{\max}(r)$ (Eq. (5)), the maximum level of nutrient in the chemostat (i.e. nutrient input $N_0$) allows hosts with a smaller size than 1µm to reach their maximal growth rate. Above that size, the host growth rate is strongly limited by the nutrient concentration in the chemostat, leading to two main observations for host size higher than 1µm: (i) a narrow area of coexistence and (ii) a significant differences between plastic and nonplastic cases (i.e. cases 2, 3, 4 and 7 are realized, see Fig. 2).

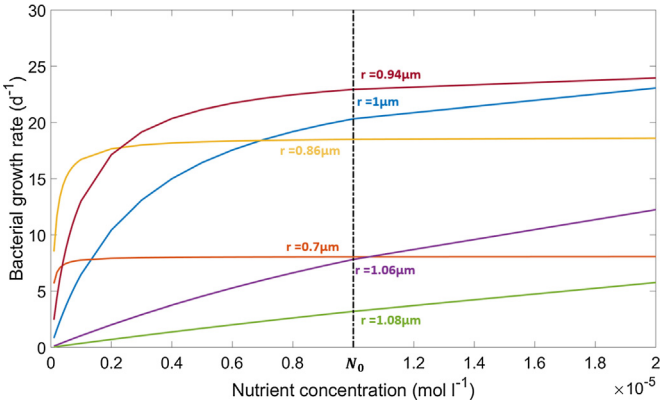


**Fig. B.1.** Monod growth curves for different bacterial sizes, considering the relationship in Eq. (6) and the allometry in Eq. (5). Color version online.

For the sake of generality, we tested two changes in the expression for the half-saturation constant: (i) the use of Eq. (6) with a value for $K_{ref}$ that is eight times bigger than its original value, and (ii) a new expression to replace Eq. (6), $K_n(r) =$

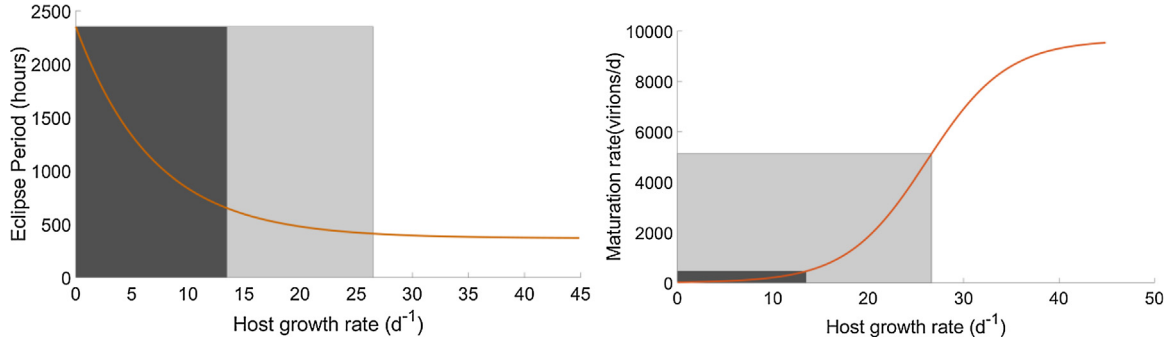


**Fig. A.1.** Example of the range of variation for the eclipse period (left) and the maturation rate (right) for a host size of 0.5µm (dark grey area) and 1 µm (clear grey area). Color version online.

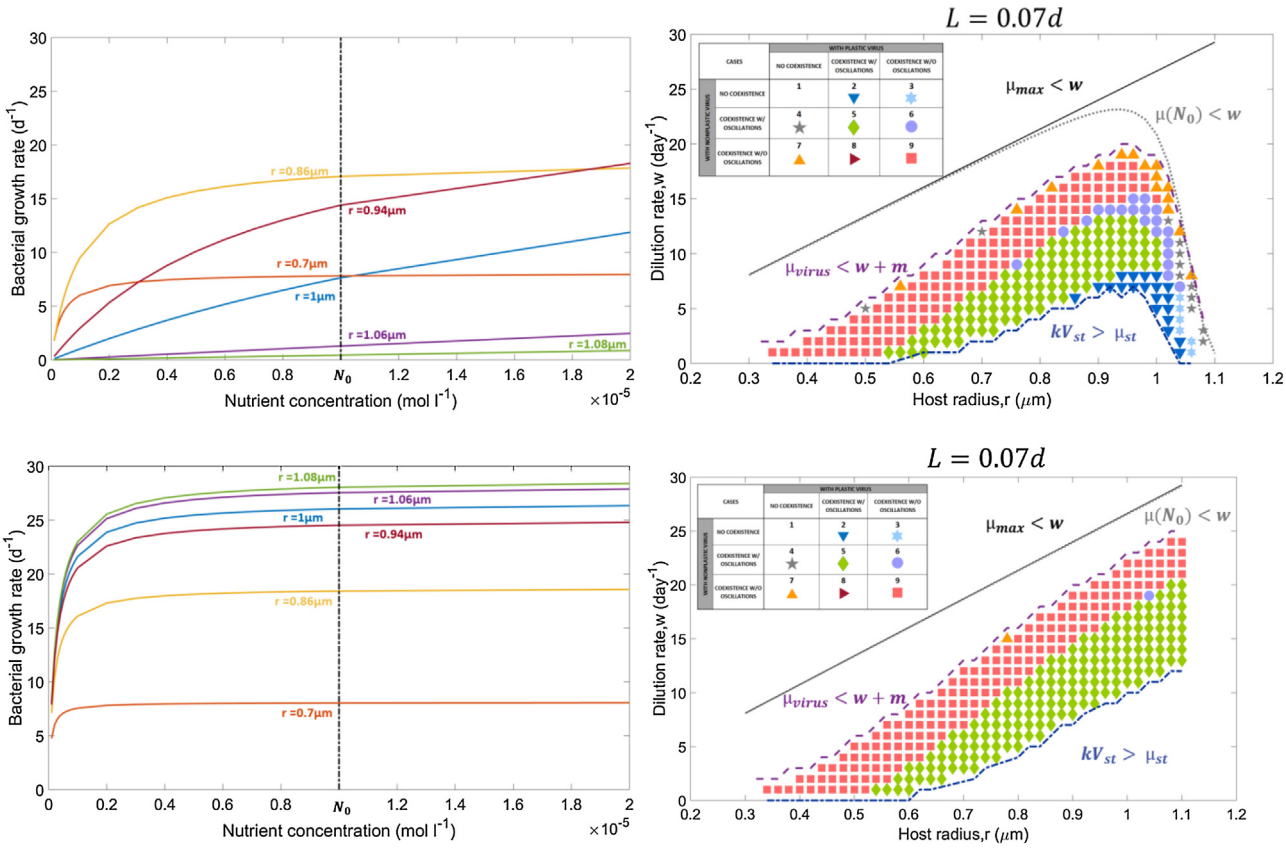


**Fig. B.2.** Growth curves (left) and coexistence areas (right) observed when: (top) increasing $K_{ref}$ in Eq. (6) by a factor 8 and (bottom) Eq. (6) is replaced by the marine-phytoplankton-based allometry $K_n(r) = 10^{-6}10^{-0.84+0.33log_{10}(4\pi r^3/3)}$ (Edwards et al 2012). Color version online.

$10^{-6}10^{-0.94+0.33\ log_{10}(\frac{4\pi r^3}{3})}$ which originates from marine phytoplankton (with nitrogen as focal nutrient, see Edwards et al. 2012)). The former option (Eq. ((6) with a much higher $K_{ref}$) shows that host with sizes smaller than the previous limit (1µm) cannot reach maximal growth for $N \leq N_0$. As a consequence, the coexistence area shifts towards lower values of the host size (see Fig. B.2, upper panels). For the latter option (new expression for $K_n(r)$) and contrarily with observations with Eq. (6), any host size can reach its $\mu_{\max}$ for $N \leq N_0$, leading to the loss of some of the behaviour observed with Eq. (6) (see Fig. B.2, bottom panels). Because keeping host maximal growth rates equalizes the traits associated with the plastic and nonplastic versions of the model, the variation in the range of host sizes that reach maximal growth rates affects the observation of cases such as 2-4 and 6-8: a wider range of host sizes reaching maximal growth rates reduces differences between plastic and nonplastic models, which entails a loss of cases. None of these changes, however, altered qualitatively the sequence of behaviours observed as the dilution rate increases (as described in Fig. 3).

## C. Supplementary figures

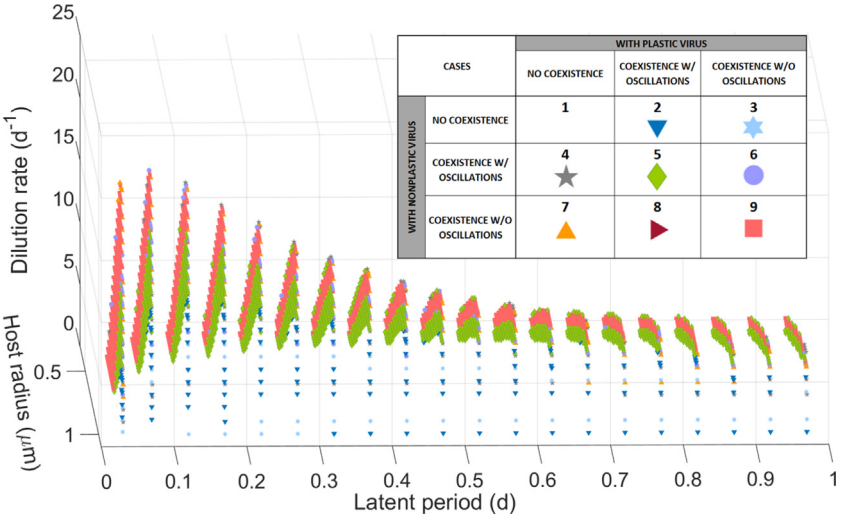


**Fig. C.1.** Region of coexistence in the 3D space (latent period, host radius, dilution rate) where the legend of each symbol/colour is represented in the right corner. Color version online.

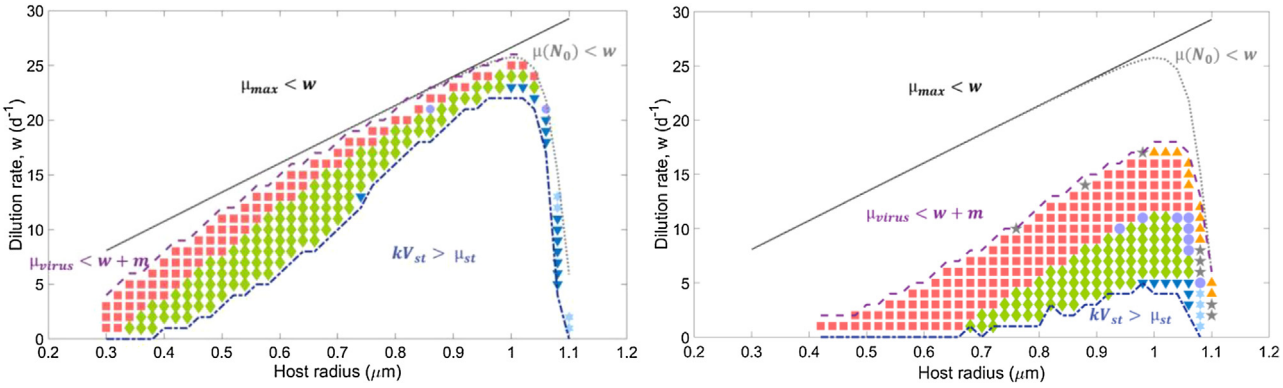


**Fig. C.2.** Slice of the region of coexistence for L=0.07d for different crowding strength. Left: for $\alpha = 5 \times 10^{-9}$ d cell$^{-1}$. Right: for $\alpha = 200 \times 10^{-9}$d cell$^{-1}$. The legend of each symbol/colour as in Fig. C.1.

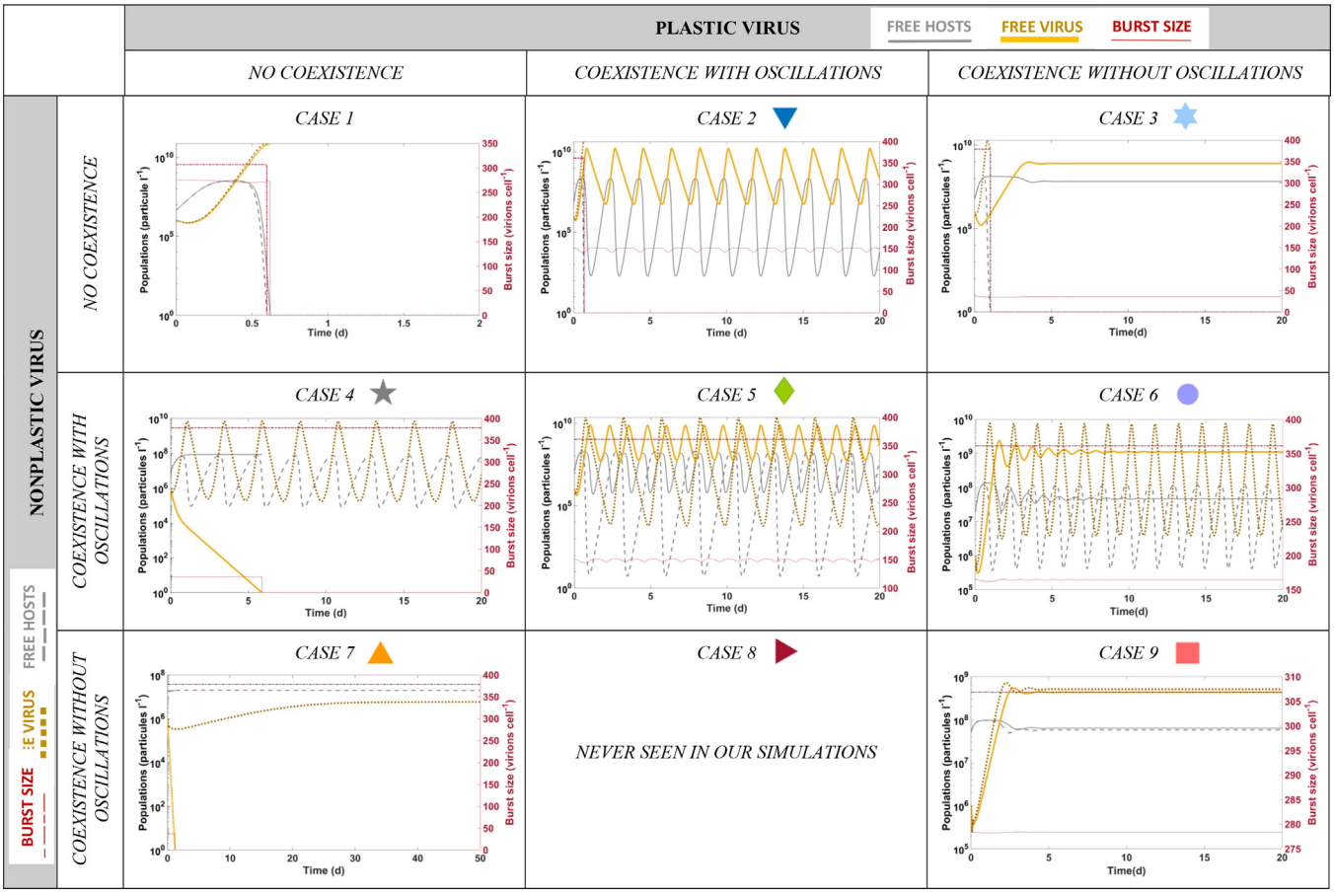


**Fig. C.3.** Examples of the dynamical profiles of the possible outcomes for plastic and nonplastic models. Color version online.

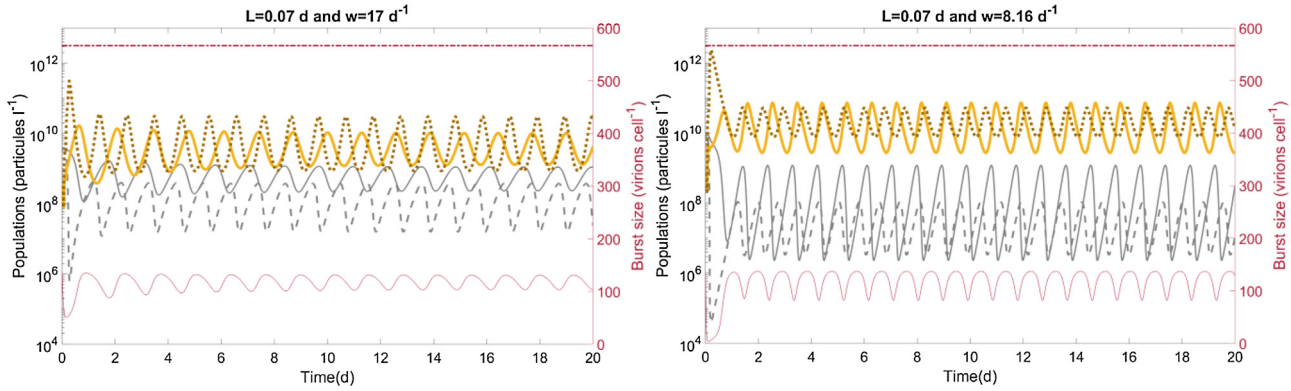


**Fig. C.4.** Dynamics for the host population density (grey), virus population density (yellow), and burst size (red) for the system described with the plastic viral model (solid lines) and nonplastic model (dashed lines), in a system in which an additional input of hosts is included (additional hosts included at the same rate as dilution, $w \bullet C_0$, with $C_0=10^7$ cells/l). For both panels, the crowding effect was eliminated (i.e. $\alpha=0$) and the input nutrient was increased to $N_0=10^{-4}$ mol/l. The nonplastic virus, due to its high performance (see text), shows a much higher burst size than the plastic one. When the dilution rate is high (left panel), the relative amplitude shown by the populations of plastic and nonplastic models is similar to that observed in Fig. C.3 case 5 (i.e. plasticity dampens oscillations). For low dilution rates (right panel), however, the oscillations for the populations in the plastic model show the larger amplitude. Color version online.

## References


Abedon, S.T., 1989. Selection for bacteriophage latent period length by bacterial density: A theoretical examination. Microbial Ecol. 18 (2), 79–88.

Abedon, S.T., 2009. Phage evolution and ecology. Adv. Appl. Microbiol. 67, 1–45.

Abedon, S.T., Hyman, P., Thomas, C., 2003. Experimental examination of bacteriophage latent-period evolution as a response to bacterial availability. Appl. Environ. Microbiol. 69 (12), 7499–7506.

Abedon, S.T., Herschler, T.D., Stopar, D., 2001. Bacteriophage latent-period evolution as a response to resource availability. Appl. Environ. Microbiol. 67 (9), 4233–4241. doi:10.1128/AEM.67.9.4233-4241.2001.

Beretta, E., Kuang, Y., 1998. Modeling and analysis of a marine bacteriophage infection. Math Biosci. 149 (1), 57–76.

Berg, H.C., Purcell, E.M., 1977. Physics of chemoreception. Biophys. J. 20 (2), 193–219. doi:10.1016/S0006-3495(77)85544-6.

Birch, E.W., Ruggero, N.A., Covert, M.W., 2012. Determining host metabolic limitations on viral replication via integrated modeling and experimental perturbation. PLoS Comput. Biol. 8 (10), e1002746.

Bonachela, J.A., Raghib, M., Levin, S.A., 2011. Dynamic model of flexible phytoplankton nutrient uptake.. In: Proceedings of the National Academy of Sciences, 108, pp. 20633–20638. doi:10.1073/pnas.1118012108.

Bratbak, G., Egge, J.K., Heldal, M., 1993. Viral Mortality of the Marine Alga Emiliania Huxleyi (Haptophyceae) and Termination of Algal Blooms. Marine Ecology Progress Series.

Breitbart, M., 2012. Marine Viruses: Truth or Dare, 4. Annual Review of Marine Science.

Brussaard, C.P.D., 2004. Viral Control of Phytoplankton Populations—a Review1. J. Eukaryot. Microbiol. 51 (2), 125–138. doi:10.1111/j.1550-7408.2004.tb00537.x.

Calendar, R.L., Abedon, S.T., 2005. The Bacteriophages. Oxford University Press.

Choua, M., Bonachela, J.A., 2019. Ecological and evolutionary consequences of viral plasticity. Am. Natural. 193 (3), 346–358. doi:10.1086/701668.

Delbrück, M., 1940. Adsoprtion of bacteriophage under various physiological conditions of the host. J. Gen. Physiol. 23 (5), 631–642.

Edwards, K.F., Steward, G.F., 2018. Host traits drive viral life histories across phytoplankton viruses. Am. Natural. 191 (5), 566–581.

Edwards, K.F., Thomas, M.K., Klausmeier, C.A., Litchman, E., 2012. Allometric scaling and taxonomic variation in nutrient utilization traits and maximum growth rate of phytoplankton. Limnol. Oceanogr. 57 (2), 554–566. doi:10.4319/lo.2012.57.2.0554.

edited by Fuhrman, J., 1992. Bacterioplankton Roles in Cycling of Organic Matter: The Microbial Food Web. In: Paul, G.Falkowski, Avril, D.Woodhead, Katherine, Vivirito (Eds.), Primary Productivity and Biogeochemical Cycles in the Sea. Springer, Boston, MAUS, pp. 361–383 edited by.

Fuhrman, J.A., 1999. Marine viruses and their biogeochemical and ecological effects. Nature 399 (6736), 541–548.

Fuhrman, J.F., McManus, G.B., 1984. Do bacteria-sized marine eukaryotes consume significant bacterial production? Sciences 224 (4654), 1257–1260.

Füchslin, H.P., Schneider, C., Egli, T., 2012. In glucose-limited continuous culture the minimum substrate concentration for growth, s(min), is crucial in the competition between the enterobacterium Escherichia coli and Chelatobacter heintzii, an environmentally abundant bacterium. ISME J. 6 (4), 777–789. doi:10.1038/ismej.2011.143.

Gaedke, U., Hochstädter, S., Straile, D., 2002. Interplay between energy limitation and nutritional deficiency: empirical data and food web models. Ecolog. Monogr. 72 (2), 251–270.

Gallet, R., Violle, C., Fromin, N., Jabbour-Zahab, R., Enquist, B.J., Lenormand, T., 2017. The evolution of bacterial cell size: the internal diffusion-constraint hypothesis. ISME J 11 (7), 1559–1568. doi:10.1038/ismej.2017.35.

Gibert, J., Delong, J., 2015. Individual Variation Decreases Interference Competition but Increases Species Persistence. 52, doi: 10.1016/bs.aecr.2015.01.002.

Gnezda-Meijer, K., Mahne, I., Poljsak-Prijatelj, M., Stopar, D., 2006. Host physiological status determines phage-like particle distribution in the lysate. FEMS Microb. Ecol. 55 (1), 136–145.

Golec, P., Karczewska-Golec, J., Łoś, M., Węgrzyn, G., 2014. Bacteriophage T4 can produce progeny virions in extremely slowly growing Escherichia coli host: comparison of a mathematical model with the experimental data. FEMS Microbiol. Lett. 351 (2), 156–161. doi:10.1111/1574-6968.12372.

Hoverman, J.T., 2010. Predator-induced Plasticity. eLS 67, 309–318. doi:10.1002/9780470015902.a0003305.pub2.

Levin, B.R., Stewart, F.M., Chao, L., 1977. Resource-Limited Growth, Competition, and Predation: A Model and Experimental Studies with Bacteria and Bacteriophage. Am. Natural. 111 (977), 3–24. doi:10.1086/283134.

Litchman, E., Klausmeier, C.A., Schofield, O.M., Falkowski, P.G., 2007. The role of functional traits and trade-offs in structuring phytoplankton communities: scaling from cellular to ecosystem level. Ecol Lett. 10 (12), 1170–1181. doi:10.1111/j.1461-0248.2007.01117.x.

Loferer-Krößbacher, M., Klima, J., Psenner, R., 1998. Determination of bacterial cell dry mass by transmission electron microscopy and densitometric image analysis. Appl. Environ. Microbiol. 64 (2), 688–694.

Lomas, M.W., Bonachela, J.A., Levin, S.A., Martiny, A.C., 2014. Impact of ocean phytoplankton diversity on phosphate uptake. Proc. Natl. Acad. Sci. USA 111 (49), 17540–17545. doi:10.1073/pnas.1420760111.

Maat, D.S., van Bleijswijk, J.D., Witte, H.J., Brussaard, C. P., 2016. Virus production in phosphorus-limited Micromonas pusilla stimulated by a supply of naturally low concentrations of different phosphorus sources, far into the lytic cycle. 92 (9), doi: 10.1093/femsec/fiw136.

Monod, J., 1949. The growth of bacterial cultures. Ann. Rev. Microbiol. 3 (1), 371–394. doi:10.1146/annurev.mi.03.100149.002103.

Mougi, A., Kishida, O., 2009. Reciprocal phenotypic plasticity can lead to stable predator-prey interaction. J. Animal Ecol. 78 (6), 1172–1181.

Nikaido, H., Vaara, M., 1985. Molecular basis of bacterial outer membrane permeability. Microbiol. Rev. 49 (1), 1–32.

O'Malley, M.A., 2016. The ecological virus. Stu. History Philos. Sci. Part C Stud. History Philos. Biolog. Biomed. Sci. 59.

Rabinovitch, A., Fishov, I., Hadas, H., Einav, M., Zaritsky, A., 2002. Bacteriophage T4 development in Escherichia coli is growth rate dependent. J. Theor. Biol. 216 (1), 1–4. doi:10.1006/jtbi.2002.2543.

Ramanculov, E., Young, R., 2001. Genetic analysis of the T4 holin: timing and topology. Gene 265 (1-2), 25–36.

Ramos-Jiliberto, R., Duarte, H., Frodden, E., 2008. Dynamic effects of inducible defenses in a one-prey two-predators system. Ecolog. Model. 214 (2), 242–250. doi:10.1016/j.ecolmodel.2008.02.004.

Schulze, K.L., Lipe, R.S., 1964. Relationship between substrate concentration, growth rate, and respiration rate of Escherichia coli in continuous culture. Archiv für Mikrobiol. 48 (1), 1–20. doi:10.1007/bf00406595.

Schwartz, M., 1976. The adsorption of coliphage lambda to its host: effect of variations in the surface density of receptor and in phage-receptor affinity. J. Molecul. Biol. 103, 521–536.

Servais, P., Billen, G., Rego, J.V., 1985. Rate of Bacterial mortality in aquatic environments. Appl. Environ. Microbiol. 49 (6), 1448–1454.

Sherr, E.B., Pedrós-Alió, C., 1989. Simultaneous measurement of bacterioplankton production and protozoan bactivory in estuarine water 54. doi:10.3354/meps054209.

Shestopaloff, Y. K. 2016. "Interspecific allometric scaling of unicellular organisms as an evolutionary process of food chain creation." arXiv preprint arXiv:1611.09824.

Suttle, C.A., 2007. Marine viruses — major players in the global ecosystem. Nature Rev. Microbiol. 5 (10), 801. doi:10.1038/nrmicro1750.

Thyrhaug, R., Larsen, A., Thingstad, T.F., Bratbak, G., 2003. Stable Coexistence in Marine Algal Host-Virus Systems 254.
Walsh, D., Mohr, I., 2011. Viral subversion of the host protein synthesis machinery. Nature Rev. Microbiol. 9 (12), 860–875.
Wang, I., 2006. Lysis timing and bacteriophage fitness. Genetics 172 (1), 17–26. doi:10.1534/genetics.105.045922.
Wang, I., Smith, D.L., Young, R., 2000. Holins: The protein clocks of bacteriophage infections. Ann. Rev. Microbiol. 54 (1), 799–825. doi:10.1146/annurev.micro.54.1.799.
Wang, Z., Goldenfeld, N., 2010. Fixed points and limit cycles in the population dynamics of lysogenic viruses and their hosts. Phys. Rev. E, Statist. Nonlinear, Soft Matter Phys. 82 (1 Pt 1), 011918. doi:10.1103/physreve.82.011918.
Weinbauer, M.G., 2004. Ecology of prokaryotic viruses. FEMS Microbiol. Rev. 28, 127–181.
Weitz, J.S., Dushoff, J., 2008. Alternative stable states in host–phage dynamics. Theoret. Ecol. 1 (1), 13–19. doi:10.1007/s12080-007-0001-1.
Wirtz, Kai W., 2002. A generic model for changes in microbial kinetic coefficients. J. Biotechnol. 97 (2), 147–162.
Yamamichi, M., Yoshida, T., Sasaki, A., 2011. Comparing the effects of rapid evolution and phenotypic plasticity on predator-prey dynamics. Am. Natural. 178 (3), 287–304. doi:10.1086/661241.
You, L., Suthers, P., Yin, J., 2002. Effects of Escherichia coli physiology on growth of phage T7 in vivo and in silico. J. Bacteriol. 184 (7), 1888–1894.
Young, R., Bläsi, U., 1995. Holins: form and function in bacteriophage lysis. FEMS Microbiol. Rev. 17 (1), 191–205. doi:10.1016/0168-6445(94)00079-4.